Geochemistry Geophysics Geosystems G3

Published by AGU and the Geochemical Society

Article
Volume 14, Number 2
28 February 2013
doi:10.1002/ggge.20072
ISSN: 1525-2027

Numerical modeling of geochemical variations caused by crustal relamination

Katharina Vogt
Geophysical Fluid Dynamics Group, Institute of Geophysics, Department of Earth Sciences, Swiss Federal Institute of Technology (ETH-Zurich), Sonneggstrasse, 5, 8092 Zurich, Switzerland (katharina.vogt@erdw.ethz.ch)

Antonio Castro
Experimental Petrology Associate Unit. CSIC-Universidad de Huelva., Campus del Carmen, Huelva, Spain

Taras Gerya
Geophysical Fluid Dynamics Group, Institute of Geophysics, Department of Earth Sciences, Swiss Federal Institute of Technology (ETH-Zurich), Sonneggstrasse, 5, 8092 Zurich, Switzerland

Department of Geology, Moscow State University, Moscow, Russia

[1] Geochemical consequences of composite diapirs formed in subduction zones have been studied using a thermomechanical numerical model of an ocean-continent subduction zone. This model includes dehydration of subducted crust, aqueous fluid transport, partial melting, and melt emplacement. Subduction of crustal material to sublithospheric depth results in the formation of a tectonic rock mélange composed of basalt, sediment, and hydrated /serpentinized mantle. At asthenospheric depth, this rock mélange may evolve into partially molten diapirs and rise through the mantle prior to emplacement (relamination) at crustal levels. We have investigated the composition and the geochemical evolution of liquids derived from such composite diapirs by analyzing the differing proportions of the crustal end-members in the source, i.e., basalt and sediment. Our results show that the proportions of the components (in the diapiric mélange) are limited to short-range variations within an interval of X_b [=volume fraction of basalt/(basalt + sediment)] = 0.4 – 0.8, yielding melt with a relatively stable granodioritic major element composition. Hence, granodioritic melt is transported by rising composite diapirs to crustal levels, contributing to the growth of the continental crust. In addition to this, we have calculated Sr and Nd isotopic initial ratios of the diapiric mélange as a function of time, based on the fraction of the components in the mélange. Liquids derived from composite diapirs inherit the geochemical characteristics of the composite source and show distinct temporal variations of radiogenic isotopes depending on the changing values of X_b. Partial melting of composite diapirs is therefore expected to produce melt with a constant major element composition but substantial changes in terms of radiogenic isotopes.

Components: 11,400 words, 6 figures, 4 tables.

Keywords: subduction zone; continental crust; relamination; composite diapir; crustal growth; isotopic variations.

Index Terms: 0545 Modeling: 1952 Modeling; 4255 Numerical modeling; 4316 Physical modeling; 1020 Composition of the continental crust

Received 21 November 2012; **Revised** 15 January 2013; **Accepted** 15 January 2013; **Published** 28 February 2013.

Vogt K., A. Castro, and T. Gerya (2013), Numerical modeling of geochemical variations caused by crustal relamination, *Geochem. Geophys. Geosyst.*, *14*, 470–487, doi:10.1002/ggge.20072.

1. Introduction

[2] The continental crust is believed to have formed by melting and geochemical fractionation of the mantle [*Hofmann*, 1988]. Although it is unclear if continents have grown with time [*Taylor and McLennan*, 1985; *McCulloch and Wasserburg*, 1978] or have reached a steady state by crustal recycling after formation in the Archean [*Amstrong*, 1981], isotopic data demonstrate that continental formation has been occurring throughout Earth history [*Rudnick*, 1995]. However, partial melting of the peridotite mantle produces basaltic magmas that are less evolved (i.e., poorer in silica) than the andesitic bulk composition of the crust. Accordingly, different models have been suggested to account for this differentiation: (i) partial melting of the subducted oceanic crust [*Drummond and Defant*, 1990; *Defant and Drummond*, 1990], (ii) reaction of slab-derived melts with the overlying perioditic mantle [*Ringwood and Green*, 1966; *Kelemen*, 1995; *Kelemen et al*., 2003a, *Behn et al*., 2011], and (iii) hydration and partial melting of the metazomatized mantle [e.g., *Schmidt and Poli*, 1998; *Iwamori*, 1998, *Tatsumi*, 2005] followed by intracrustal differentiation and lower crustal foundering [*Kay and Kay*, 1991]. Although foundering is probably an important mechanism in some places [*DeBari and Sleep*, 1991; *Kelemen et al*., 2003b], recent studies have shown that felsic material may also detach from the slab because of the intrinsic buoyancy of the sediment layer itself [*Currie et al*., 2007, *Behn et al*., 2011, *Hacker et al*., 2011; *Miller and Behn*, 2012] and hence modify the subarc mantle. Alternatively, hydration and partial melting atop the slab may trigger the formation of composite diapirs composed of partially molten basalt, sediment, and hydrated/serpentinized mantle [*Gerya and Yuen*, 2003; *Gerya et al*., 2006; *Gerya and Meilick*, 2011; *Zhu et al*., 2009, *Zhu et al*., 2011a, 2011b; *Vogt et al*., 2012]. Some of these latter studies were examined using laboratory experiments in terms of major element compositions and phase relations [*Castro and Gerya*, 2008, *Castro et al*., 2009; *Castro et al*., 2010; *Castro et al*., 2012a]. The cotectic behavior of liquid formed by partial melting of subducted rock mélanges at sublithospheric depths [*Castro et al*., 2010] is a prominent feature. Cotectic liquids have an almost constant composition, buffered by the solid coexisting assemblage. This phase equilibria experimental study shows, therefore, that composite diapirs are favorable for the production of silicic magmas with minor compositional variations in terms of major elements. This is consistent with the production of large silicic batholiths, composed of rocks of granodiorite to tonalite composition that yield a constant major element composition despite their long-lived magmatism [*Castro et al*., 2010 and references therein] and contribute to the growth of the continental crust [*Condie*, 1997; *Hawkesworth and Kemp*, 2006]. Geochemical (trace elements) and isotopic variations, on the other hand, are nearly independent of the major element geochemistry, and large variations in time and space have been reported for distinct geological settings, where granodioritic intrusions display a constant major element composition. These differences are generally related to (i) changes in crustal thickness with time [*Haschke et al*., 2002; *Mamani et al*., 2010] and space [*Hildreth and Moorbath*, 1988] (ii) involvement of an enriched component i.e., old lithosphere [*Rogers and Hawkesworth*, 1989] and (iii) source region contamination of the sub-arc mantle by sediment subduction, crustal erosion, and partial melting of the subducting slab [*Stern*, 1991]. Sediment subduction and crustal subduction erosion are apparent tectonic features of modern plate boundaries *von Huene and Scholl*, 1991, *von Huene and Lallemand*, 1990], and partial melting of these crustal rocks mixed with oceanic crust may account for the geochemical and isotopic variability observed in modern arc magmas. In particular, the source composition of batholiths generated at active continental margins may vary between the two end-members, namely, sediment and basaltic oceanic crust [*Castro et al*., 2010], imposing a wide variability in terms of trace elements and isotopic ratios that has not been explored yet.

[3] We have therefore undertaken a detailed study of 2-D petrological-thermomechanical numerical experiments on subduction at continental margins to (i) characterize the variability of geochemical signatures of magmas produced by composite diapirs, and (ii) investigate its implications for batholith formation.

2. Methods

2.1. Numerical Model Setup

[4] The numerical model simulates forced subduction of an oceanic plate beneath a continental margin on a lithospheric to upper mantle cross-section (4000 km by 200 km; Figure 1). The rectangular grid with 2041×201 nodal points is non-uniform and

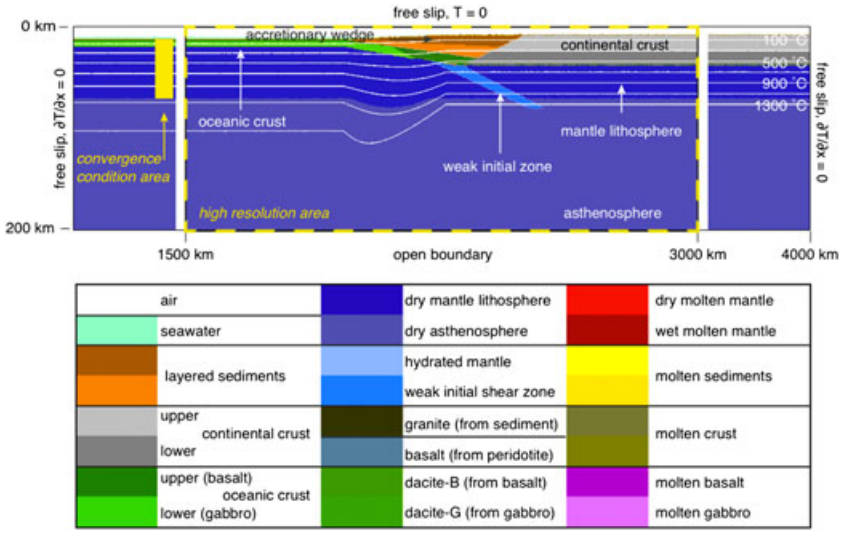

Figure 1. Initial setup of the numerical model (see section 2.1 for details). Staggered grid resolution is 2041 × 201 nodal points, with more than 10 million randomly distributed markers. Grid step is 1 × 1 km in the subduction zone area (1500–3000 km) and 5 × 1 km outside of this area. Isotherms are displayed in white for increments of 200°C, starting from 100°C. Colors indicate materials (i.e., rock type or melt), which appear in subsequent figures. To illustrate deformation, two layers with the same physical properties are distinguished using different colors for sediments, crust (upper and lower crust), and mantle (asthenosphere and lithosphere).

contains a 1500 km wide high-resolution area of 1 km × 1 km in the center of the domain, while the rest of the model remains at a lower resolution (5 × 1 km). The oceanic crust (2500 km) is pushed towards a fixed continental crust (1500 km) at an imposed convergence rate of 5 cm/year. A rheologically weak shear zone at the bottom of the oceanic-continental suture zone prescribes initiation of subduction. The oceanic crust is composed of 2 km of hydrothermally altered basalt, underlain by 5 km of gabbroic rocks that cover 2500 km horizontally. The continental crust is felsic and has a total thickness of 30 km, composed of 15 km upper and 15 km lower crust that extend over 1500 km. The total thickness of the continental crust corresponds to extended continental crust of Western Europe and Western North America (as opposed to orogens) and was adopted according to *Christensen and Mooney* [1995]. Above the trench, accretionary sediments are settled separating the continental crust from the downgoing slab. In the course of subduction, these layered sediments are exposed to erosion, sedimentation, and sediment subduction [*Gerya and Meilick*, 2011]. Both the asthenosphere and the upper mantle are composed of anhydrous peridotite and are defined by the temperature profile. The compositions and detailed material properties used for these different lithologies are given in Tables 1 and 2, respectively. Because mineralogical reactions such as phase transitions, dehydration reactions, or melting reactions may significantly affect the physical properties of rocks, stable phase relations for these different lithologies (Table 1) were computed as a function of pressure and temperature using free energy minimization [*Connolly*, 2005]. The thermodynamic

Table 1. Composition of the Lithologies Used in the Simulations

Composition (wt%)	Sediment	Basalt	Gabbro	Mantle
SiO_2	61.10	47.62	53.49	45.55
Al_2O_3	12.43	14.48	14.07	4.03
FeO	5.43	10.41	6.86	7.47
MgO	2.59	6.92	12.07	37.42
CaO	6.21	13.39	10.73	3.18
Na_2O	2.54	2.15	1.22	0.33
K_2O	2.13	0.58	0.09	0.03
H_2O	7.6	2.78	1.47	1.98

Compositions used for the calculations of stable mineral assemblages by Gibbs free energy minimization [*Connolly*, 2005] and subsequent thermodynamic properties used in the numerical experiments (i.e., water content, effective density, isobaric heat capacity, thermal expansion, adiabatic heating, latent heating, equilibrium water content, and melt content). Sediment is the GLOSS average [*Plank and Langmuir*, 1998]; basalt is an average for the upper 500 m of the igneous section of the oceanic crust [*Staudigel et al.*, 1989]; gabbro is a synthetic composition for the gabbroic section of the oceanic crust [*Behn and Kelemen*, 2003], modified to contain up to 1.5 wt% water to represent the effects of lower crustal hydrothermal alteration [*Carlson*, 2003], and peridotite is the LOSIMAG composition [*Hart and Zindler*, 1986] chosen to represent mantle peridotite. The compositions have been simplified by the omission of minor elements such as Mn, P, Ti, and Cr, and the assumption that all Fe is ferrous; additionally, CO_2 has been removed from the GLOSS sediment composition.

10.1002/ggge.20072

Table 2. Physical Properties of Rocks[1] Used in Numerical Experiments

Material	ρ_0 (kg/m^3)	k, W/(m K) (at T_K, P_{MPa})	$T_{solidus}$, K (at P_{MPa})	$T_{liquidus}$, K (at P_{MPa})	H_l (kJ/kg)	H_r (μW/m^3)
Sediments	2600 (solid) 2400 (molten)	$[0.64+807/(T+77)]\times\exp(0.00004\cdot P_{MPa})$	$889+17900/(P+54)+20200/(P+54)^2$ at $P<1200$ MPa, $831+0.06P$ at $P>1200$ MPa	$1262+0.09P$	300	1.5 1.5
Upper continental crust	2700 (solid) 2400 (molten)	$[0.64+807/(T+77)]\times\exp(0.00004\cdot P_{MPa})$	$889+17900/(P+54)+20200/(P+54)^2$ at $P<1200$ MPa, $831+0.06P$ at $P>1200$ MPa	$1262+0.09P$	300	1 1.5
Lower continental crust	2700 (solid) 2400 (molten)	$[0.64+807/(T+77)]\times\exp(0.00004\cdot P_{MPa})$	$973-70400/(P+354)+77800000/(P+354)^2$ at $P<1600$ MPa, $935+0.0035P+0.0000062P^2$ at $P>1600$ MPa	$1423+0.105P$	380	1 1.5
Upper oceanic crust (basalt)	3000 (solid) 2900 (molten)	$[1.18+474/(T+77)]\times\exp(0.00004\cdot P_{MPa})$	$973-70400/(P+354)+77800000/(P+354)^2$ at $P<1600$ MPa, $935+0.0035P+0.0000062P^2$ at $P>1600$ MPa	$1423+0.105P$	380	0.25 0.25
Lower oceanic crust (gabbro)	3000 (solid) 2900 (molten)	$[1.18+474/(T+77)]\times\exp(0.00004\cdot P_{MPa})$	$973-70400/(P+354)+77800000/(P+354)^2$ at $P<1600$ MPa, $935+0.0035P+0.0000062P^2$ at $P>1600$ MPa	$1423+0.105P$	380	0.25 0.25
Dry mantle (lithosphere – asthenosphere)	3300 (solid) 2900 (molten)	$[0.73+1293/(T+77)]\times(1+0.00004P)$	$1394+0.132899P-0.000005104P^2$ at $P<10000$ MPa $2212+0.030819(P-10000)$ at $P>10000$ MPa	$2073+0.114P$	400	0.022 0.022
Wet mantle (lithosphere-asthenosphere)	3000 (serpentinized) 3200 (hydrated) 2900 (molten)	$[0.73+1293/(T+77)]\times(1+0.00004P)$	$1240+49800/(P+323)$ at $P<2400$ MPa, $1266-0.0118P+0.0000035P^2$ at $P>2400$ MPa	$2073+0.114P$	400	0.022 0.022 0.022
Felsic magmatics from: sediments, upper crust	2600 (solid)	$[0.64+807/(T+77)]\times\exp(0.00004\cdot P_{MPa})$	$889+17900/(P+54)+20200/(P+54)^2$ at $P<1200$ MPa, $831+0.06P$ at $P>1200$ MPa	$1262+0.09P$	300	1.5
Mafic Magmatics from: basalt, gabbro, lower crust, mantle	3000 (solid)	$[1.18+474/(T+77)]\times\exp(0.00004\cdot P_{MPa})$	$973-70400/(P+354)+77800000/(P+354)^2$ at $P<1600$ MPa, $935+0.0035P+0.0000062P^2$ at $P>1600$ MPa	$1423+0.105P$	380	0.25
References [2]	1, 2	3, 9	4, 5, 6, 7, 8	4	1, 2	1

[1]Other properties (for all rock types): $Cp=1000\,J\,kg^{-1}\,K^{-1}$, $\alpha=3\times10^{-5}\,K^{-1}$, $\beta=1\times10^{-11}\,MPa^{-1}$.

[2]1 = [*Turcotte and Schubert*, 2002]; 2 = [*Bittner and Schmeling*, 1995]; 3 = [*Clauser and Huenges*, 1995]; 4 = [*Schmidt and Poli*, 1998]; 5 = [*Hess*, 1989]; 6 = [*Hirschmann*, 2000]; 7 = [*Johannes*, 1985]; 8 = [*Poli and Schmidt*, 2002]; 9 = *Hofmeister* [1999], 10 = [*Ranalli*, 1995].

database used for the properties of all end-member species and mineral solutions are summarized in *Gerya et al*., 2006. All mechanical boundary conditions are free slip; only the lower boundary is permeable, satisfying an external free slip boundary condition [*Gorczyk et al*., 2007; *Ueda et al*., 2008]. To allow for topographic buildup of the lithosphere, the top surface of the lithosphere is treated as an internal free surface [*Schmeling et al*., 2008] by using a top layer (of 8–12.5 km thickness) with low viscosity (10^{18} Pas) and low density (1 kg/m^3 for air, 1000 kg/m^3 for sea water). The initial temperature field of the oceanic plate is defined by its oceanic geotherm [*Turcotte and Schubert*, 2002] for a specific lithospheric cooling age of 40 Myr. The initial temperature field of the continental plate increases linearly from 0°C at the surface to 1367°C at the lithosphere-asthenosphere boundary at 72 km depth. For the asthenospheric mantle (>72 km), a thermal gradient of 0.5°C km^{-1} is used. This is in accordance with recent studies, where sharp lithosphere-asthenosphere boundaries have been imaged at shallow depth (~60–90 km), such as for instance beneath the western U.S. [*Levander and Miller*, 2012].

[5] The model is based on the I2VIS code [*Gerya and Yuen*, 2003] and uses conservative finite differences and a nondiffusive marker in cell technique to simulate multiphase flow. The governing conservation equations of mass, momentum, and energy and the constitutive relationship between stress and strain-rate (needed in the creeping flow regime) are solved on a staggered grid in Eulerian configuration. Conservation of mass is described by the Lagrangian continuity equation for a compressible fluid. The model includes spontaneous slab retreat and bending, dehydration of subducted crust, aqueous fluid transport, partial melting, melt extraction, and melt emplacement in the form of extrusive volcanics and intrusive plutons. For a detailed description of the governing equations and the numerical procedure employed in this study, the reader is referred to *Gerya and Yuen* [2003, 2007], and *Gerya and Meilick* [2011].

2.2. Rheology

[6] The rheologies used in this study are visco-plastic. The viscous creep of rocks is defined in terms of deformation invariants and depends on temperature, pressure, and strain rate.

[7] The viscosity for dislocation creep is defined as follows [*Ranalli*, 1995]:

$$\eta_{\text{creep}} = \frac{\dot{\varepsilon}^{\frac{1-n}{n}}}{A_D^{\frac{1}{n}}} \exp\left(\frac{E_a + PV_a}{nRT}\right)$$

where $\dot{\varepsilon} = \left(\frac{1}{2}\dot{\varepsilon}_{ij}\dot{\varepsilon}_{ij}\right)^{\frac{1}{2}}$ is the second invariant of the strain rate tensor. A_D (pre-exponential factor), E_a (activation energy), n (creep exponent), and V_a (activation volume) are experimentally determined flow law parameters, and R is the gas constant (Table 3).

[8] Plasticity is implemented using the following yield criterion, which limits the creep viscosity, altogether yielding an effective visco-plastic rheology.

$$\eta_{\text{creep}} \leq \frac{\sigma_{\text{yield}}}{2\dot{\varepsilon}_{II}}$$
$$\sigma_{\text{yield}} = c + P\sin\left(\varphi_{\text{dry}}\right)\lambda_{\text{fluid}}$$

[9] The local plastic strength of a rock depends on the mean stress, $P_{\text{total}} = P$ (dynamic pressure), ambient brittle/plastic strength c, which is the strength at $P = 0$, on the effective internal friction

Table 3. Rheology: Flow Laws[a]

Material	Flow Law	1/Ad (Pa^{n}s)	E (J/mol)	V (J/bar/mol)	n	sin(φ)	C (Pa)
Sediments	wqz	1.97×10^{17}	154×10^3	0.8	2.3	0.15	1×10^6
Upper crust	wqz	1.97×10^{17}	154×10^3	1.2	2.3	0.15	1×10^6
Lower crust	wqz	1.97×10^{17}	154×10^3	0.8	2.3	0.15	1×10^6
Basalt	wqz	1.97×10^{17}	154×10^3	0.8	2.3	0.1	1×10^6
Gabbro	plag (An75)	4.8×10^{22}	238×10^3	0.8	3.2	0.6	1×10^6
(Dry) Mantle	dry ol	3.98×10^{16}	532×10^3	0.8	3.5	0.6	1×10^6
Hydrated mantle	wet ol	5.01×10^{20}	470×10^3	0.8	4	0.6	1×10^6
Shear zone	wet ol	5.01×10^{20}	470×10^3	0.8	4	0	1×10^6
Serpentinized mantle	wet ol	5.01×10^{20}	470×10^3	0.8	4	0	1×10^6
Magmatics (all)	wqz	1.97×10^{17}	154×10^3	0.8	2.3	0.15	1×10^6

wqz = wet quartzite; plag (An75) = anorthite75; wet ol = wet olivine; dry ol = dry olivine.
[a]*Ranalli* [1995] and references therein.

angle of dry rocks, φ_{dry} and the pore fluid pressure factor λ_{fluid}. This factor is interpreted as:

$$\lambda_{fluid} = 1 - \frac{P_{fluid}}{P_{total}}$$

[10] The pore fluid pressure P_{fluid} reduces the yield strength σ_{yield} of fluid-containing porous or fractured rocks. The weakening effect of ascending melts is implemented in a similar manner. Extraction of melt decreases the yield strength σ_{yield} of rocks in the column between the area of the melt generation and emplacement, according to a prescribed melt pressure factor:

$$\lambda_{melt} = 1 - \frac{P_{melt}}{P_{total}}$$

2.3. Plate Coupling

[11] Plate coupling is a direct function of the rheological weakening effects of (i) aqueous fluids percolating from the subducting slab into the mantle wedge and (ii) melts propagating from partially molten areas formed in the mantle wedge toward the surface. Strong fluid-related weakening (low fluid pressure factor: $\lambda_{fluid} < 0.1$) promotes plate decoupling and sediment accretion, forming large growing accretionary prisms. In contrast, reduced weakening by fluids (high fluid pressure factor: $\lambda_{fluid} \geq 0.1$) results in strong coupling of the plates, leads to compression of the upper plate, and enhances sediment subduction, which results in small to medium sized accretionary prisms [*Gerya and Meilick*, 2011]. Composite diapirs formed at asthenospheric depth and thickening of the overriding plate are direct consequences. On the other hand, melt extraction from hot regions in the mantle wedge and above the slab weaken the lithosphere below the arc controlling the formation of translithospheric diapirs (diapirs that rise directly from the area of formation to the continental crust traversing the lithosphere) and underplating diapirs (diapirs that spread below the lithosphere). Where melt propagation is assumed to weaken the lithosphere (by lowering its plastic strength) sufficiently, rapid translithospheric diapir ascent is feasible (Figure 2). If, however, melt percolation has little effect on the lithospheric strength, diapiric ascent is inhibited, and the diapir spreads below the lithosphere (Figure 3).

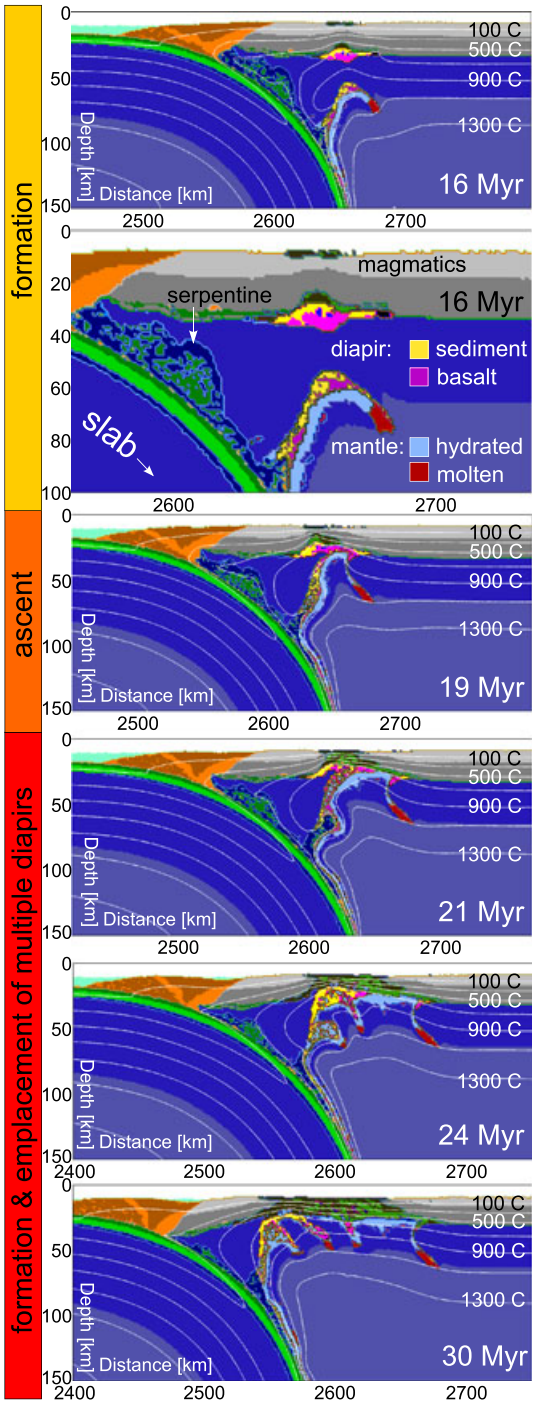

Figure 2. Translithospheric diapirs. Localization and partial melting atop the slab triggers Rayleigh-Taylor Instabilities at asthenospheric depths. Hence, composite diapirs are formed composed of sediment, basalt, and hydrated/serpentinized mantle. Rapid, buoyant ascent through the mantle is followed by emplacement at crustal levels. Continuous supply of crustal material atop the slab promotes the recurrent formation of composite diapirs.

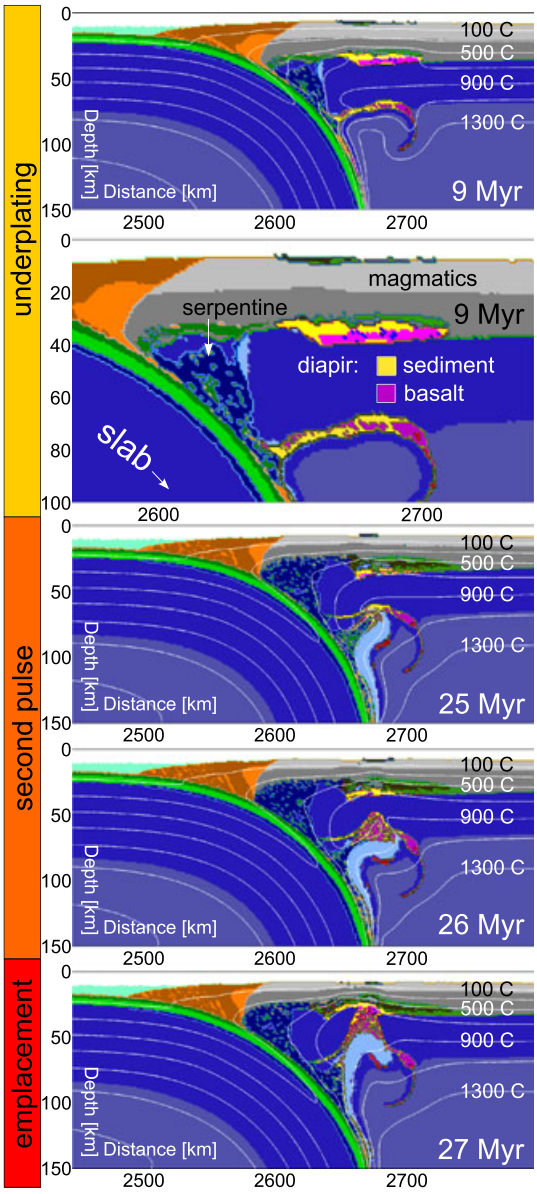

Figure 3. Underplating diapirs. Partial melting of crustal material atop the slab enables the formation of composite diapirs at asthenospheric depth. Once a diapir of high volume is formed, it detaches from the slab, and no more material is added (for up to 20 Myr). Because of the strong continental lithosphere, diapir ascent is inhibited, and the diapir underplates the continental crust for up to 20 Myr until a final upwelling (magma pulse) enables emplacement at crustal levels.

2.4. Geochemical Evaluation of Composite Diapirs

[12] We have calculated the isotopic initial ratios of Sr and Nd in the mélange (magma source) at any given time during the simulations according to a simple mass balance equation [*Faure*, 2001]:

$$\mathrm{Ri(m)} = \mathrm{Ri(b)} \times [\mathrm{i}]\mathrm{b} \times X_b + \mathrm{Ri(s)} \times [\mathrm{i}]\mathrm{s} \times (1 - X_b)$$

Ri = isotopic initial ratio of Sr or Nd, i.e., $(^{87}Sr/^{86}Sr)_{initial}$ and $(^{143}Nd/^{144}Nd)_{initial}$, calculated at the time of magma generation.

m = mélange; b = basalt; s = sediment
[i] = Concentration in ppm of Sr or Nd
X_b = fraction of basalt in the mélange

[13] The isotopic initial ratios of the mélange (Ri(m)) depend on the isotopic ratios of the components (Ri(b), Ri(s)), the element abundances of Sr and Nd in the components (basalt: [i]b, sediment: [i]s in ppm), and the fraction of the components in the mixture/source (X_b). Our numerical simulations provide the latter parameter (X_b). The initial ratios and concentrations of Sr and Nd in basalt and sediment are summarized in Table 4 and were assumed to be constant. In addition to this, we assume the following: (i) no fractionation of radiogenic isotopes (Sr, Nd) during melting or magma evolution and (ii) isotope homogenization in the source.

[14] In natural settings, crustal subduction erosion by which crustal/continental material is scrapped off the upper plate to be subducted and mixed with oceanic crust and sediment from the accretionary prism will affect the isotopic evolution of the system. However, this process is strongly dependent on the tectonic and chemical setting considered and is therefore difficult to assess. Accordingly, we assume that isotopic ratios of all crustal components (continental crust and sediment) are represented by terrigeneous sediment (Table 4).

[15] Hybridization of the mélange with the surrounding mantle was calculated in a similar manner:

$$\mathrm{Ri(hybrid)} = \mathrm{Ri(mantle)} \times [\mathrm{i}]\mathrm{mantle} \times X_{\mathrm{mantle}} + \mathrm{Ri(m)} \times [\mathrm{i}]\mathrm{mantle} \times (1 - X_{\mathrm{mantle}}).$$

[16] Ri(hybrid) represents the isotopic ratio of the parental magma (i.e., partially molten diapiric mélange)

Table 4. Initial Ratios and Concentrations of Sr and Nd in Sediment, Basalt, and Mantle

	Sediment	MORB N-MORB	Mantle CHUR
Nd (ppm)	35	6	-
Sr (ppm)	142	94	21
$^{143}Nd/^{144}Nd$	0.5120	0.5128	0.7045
$^{87}Sr/^{86}Sr$	0.72	0.7020	-
	1	2	3

1, *Taylor and McLennan* [1985]; 2, *Klein* [2003]; 3, *Sun and McDonnough* [1989].

after reaction with the mantle. X_{mantle} corresponds to the mass fraction of mantle involved in the reaction and was varied from $X_{mantle} = 0.8–0.95$ to ensure equilibrium between melt and mantle. Isotopic ratios and element abundances (Nd and Sr in ppm) of the primordial mantle are summarized in Table 4.

[17] The following assumptions have been made concerning the geochemistry of composite diapirs, composed of subducted oceanic crust and sediment. The oceanic crust is relatively homogeneous in major element composition (Mid-Ocean-Ridge-Basalt MORB are among the most homogeneous rocks on Earth in terms of major elements), but differences in trace element compositions are significant between normal, transitional, and primitive MORB. We have chosen N-MORB to represent the composition of the oceanic crust because the other two types form oceanic plateaus (T-MORB) and sea mounts (P-MORB and E-MORB), which are less abundant and may not represent the average oceanic crust. Sedimentary material, on the other hand, displays a wide variety of trace element patterns, which makes data selection more difficult. Nevertheless, greywackes are the most abundant terrigenous sediments found in flysch-type synorogenic sedimentary basins (at continental margins) and were chosen to represent the composition of subducted sediment and crustal material (Table 4).

[18] Our simplified geochemical assumptions are aimed at evaluating first-order influences on the geochemistry of melt derived from partially molten composite diapirs. Compositional changes within the diapir are related to differing proportions of basalt and sediment that will affect the geochemical evolution of melt derived from such sources.

3. Results

3.1. Dynamics of Diapir Formation

[19] Because of the large thermal contrast between the leading edge of the subducting slab and the overlying mantle, partial melting of the oceanic crust occurs shortly after subduction initiation (<5 Myr). Aqueous fluids propagate from the subducting slab into the mantle wedge, hydrating the overlying mantle. Such fluids may either form a serpentinized channel at shallow slab interfaces (<130 km) within the colder lithospheric portion of the mantle wedge or generate subsolidus metasomatism at greater depth where the mantle is hotter. Where these fluids encounter the wet mantle solidus, they induce partial melting of the hydrated mantle, enabling basaltic melt production. In contrast, localization along the slab interface and forced return flow of material within the serpentinized layer enable the formation of a complex tectonic rock mélange, composed of sediment, basalt, and hydrated/serpentinized mantle. The large density contrast (400–600 kg/m^3, depending on composition and degree of melting) between this layer and the overlying mantle wedge finally induces Rayleigh-Taylor instabilities atop the slab. Composite diapirs are formed that enable buoyant ascent of crustal material towards shallower levels of the continental lithosphere (Figures 2 and 3). Because of the differing proportions of the components in the source (i.e., basalt and sediment), the composition of these diapiric structures changes with time. Both sediment and basalt are carried into the subduction zone by the downgoing slab and form an inexhaustible source of crustal components. Their relative proportions are a result of the tectonic setting and are not imposed by the model design [*Gerya and Meilick*, 2011; *Vogt et al*., 2012]. In particular, the relative proportion of sediment and basalt is strongly dependent on the rheological plate coupling. Strong plate coupling promotes compression of the upper plate and enhances sediment subduction, whereas low coupling leads to upper plate extension and sediment accretion, forming large growing accretionary prisms [*Gerya and Meilick*, 2011]. Melt extracted from all molten components (atop the slab and inside the diapir) forms new volcanic crust at the surface and intrusive plutons at deeper crustal levels. Depending on the magnitude of melt weakening effects on the overlying lithosphere, either translithospheric (Figure 2) or underplating diapirs (Figure 3) will form. Where melt propagation is assumed to weaken the lithosphere (by lowering its plastic strength), rapid translithospheric diapir ascent is feasible (Figure 2). If, however, melt percolation has little effect on the lithospheric strength, diapiric ascent is inhibited, and the diapir spreads below the lithosphere (Figure 3).

3.2. Multiple Translithospheric Diapirs

[20] The incubation period (0–13 Myr) of translithospheric diapirs is characterized by large fluctuations in the basalt fraction (X_b = basalt/(basalt + sediment) = 1–0.3) and an overall decrease in basaltic components (Figure 4a). Localization at the slab interface and slab melting at early stages of subduction introduces large amounts of partially molten basalt into the (low viscosity) subduction channel. Progressive sediment subduction and sediment erosion eventually decrease

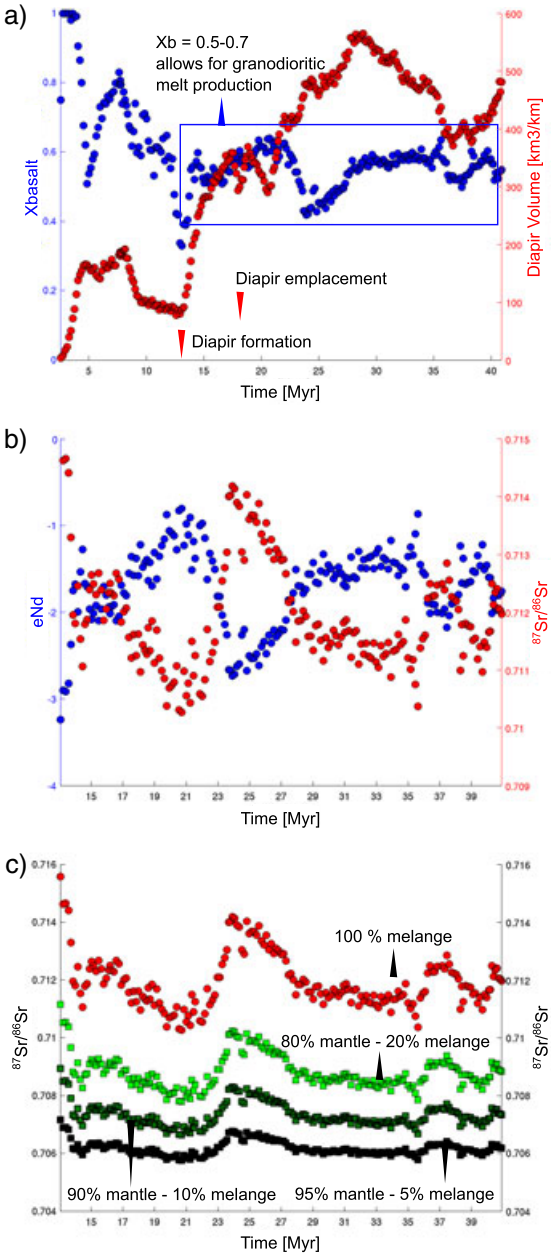

Figure 4. Isotopic variations caused by translithospheric diapirs. (a) compositional variations related to differing material inputs of basalt and sediment (X_b = basalt/(basalt + sediment) (blue dots) in relation to diapir growth (red dots). (b) Isotopic variations of liquid/melt derived from composite diapirs, based on the mass fraction of sediment and basalt (i.e., X_b) in the source (diapir). $^{87}Sr/^{86}Sr$ initial ratios are shown in red, εNd ratios are displayed in blue. An increase in basaltic components leads to an increase in εNd and a decrease in $^{87}Sr/^{86}Sr$. The recurrent supply of magma of varying composition (X_b) leads to periodic variations. (c) $^{87}Sr/^{86}Sr$ initial ratios of melt derived from composite diapirs after reactions with the mantle, shown for various melt-mantle fractions.

the basalt fraction to a minimum of $X_b = 0.3$ (Figure 4a). This enables daipir formation (Figure 2), increasing the volume of partially molten material from 80 km^3/km to 350 km^3/km (Figure 4a). Diapiric ascent is triggered, and crustal material is transported throughout the hot mantle at speeds of 1.2 cm/year (13–18 Myr). Emplacement of these partially molten structures at crustal levels results in large growing magma chambers at mid- to upper crustal levels. In spite of the rapid ascent, lower parts of the diapiric structure ("diapir tail") remain attached to the slab, forming a weak zone, composed of partially molten rock and hydrated mantle. This, in turn, enables new material to be added at its base. Hence, the diapir grows, reaching volumes of 550 km^3/km (Figure 4). New incoming magma promotes further diapir formation resulting in multiple magma pulses (on a 1–5 Myr timescale) and diapir emplacement (Figure 2). During this period of time, the basalt fraction is limited to values of $X_b = 0.4$ to 0.8 and exhibits periodic variations, which reflect the recurrent supply of magma of varying composition (Figure 4a). After 28 Myr, magmatic addition reaches a steady state, the diapir detaches from the slab, and no more magma is added to its base for the next 10 Myr at which the basalt ratio remains fixed at $X_b = 0.55$. The volume of the diapir declines from about 600 km^3/km to 400 km^3/km because of melt extraction. Finally, an upwelling is formed (~38 Myr), and additional material (100 km^3/km) is added, but the basalt fraction shows little variations (Figure 4a).

3.3. Single Underplating Diapir

[21] The basalt ratio decreases rapidly during the incubation period (0–5 Myr) form $X_b = 1$ to 0.5 until a composite diapir of high volume is formed (Figure 5a). Shortly after (8 Myr), the volume of the diapir reaches its maximum of ~500 km^3/km, and no more material is added. The diapir detaches from the slab and underplates the lithosphere for up to 20 Myr, not able to penetrate through the lithosphere (Figure 3). During this period (8 Myr–25 Myr), the basalt ratio remains limited to $X_b = 0.7$–0.5, revealing periodic variations on a 10 Myr timescale (Figure 5a). Melt extracted from the composite diapir travels through the mantle and forms volcanics at the surface and flattened intrusions in the lower crust. Thus, the volume of the diapir decreases from 300 km^3/km to 200 km^3/km (Figure 5a), and percolating melt weakens the lithosphere. Because of the constant supply of sediment and basalt at the slab interface, the diapir finally detaches (24 Myr) after

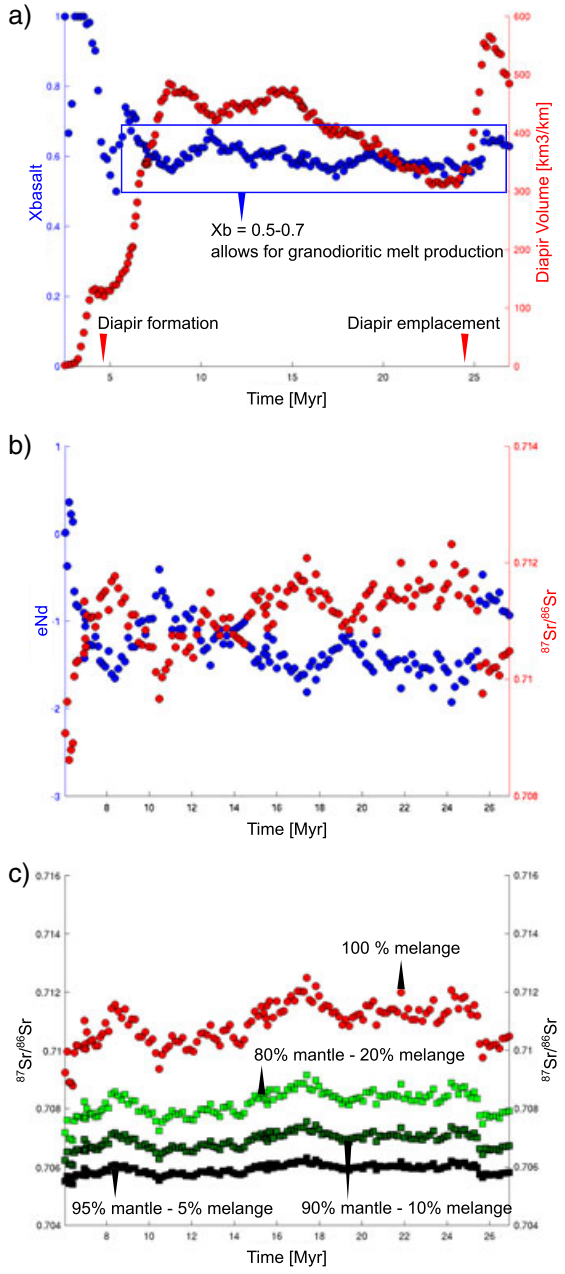

Figure 5. Isotopic variations caused by underplating diapirs. (a) compositional variations related to differing material inputs of basalt and sediment (X_b = basalt/(basalt + sediment) (blue dots) in relation to diapir growth (red dots). (b) Isotopic variations of liquid/melt derived from composite diapirs, based on the mass fraction of sediment and basalt (i.e., X_b) in the source (diapir). $^{87}Sr/^{86}Sr$ initial ratios are shown in red, εNd ratios are displayed in blue. An increase in basaltic components leads to an increase in εNd and a decrease in $^{87}Sr/^{86}Sr$. The limited supply of new magma to the source (diapir) leads to minor but distinct variations in isotopic ratios. (c) $^{87}Sr/^{86}Sr$ initial ratios of melt derived from composite diapirs after reactions with the mantle, shown for various melt-mantle fractions.

a second upwelling is formed and emplaces at crustal levels shortly after (25 Myr) (Figure 3).

4. Discussion and Geochemical Implications

4.1. Formation of Composite Diapirs

[22] Observations along active continental margins have revealed that sediments and small crustal bodies can be scrapped off the downgoing slab to form large accretionary prisms [*Von Huene and Scholl*, 1991, *Cloos and Shreve*, 1988]. Crustal material can bypass the accretionary wedge, as it remains attached to the oceanic crust, or be removed from the upper plate in the process of crustal erosion [*Von Huene and Scholl*, 1991; *Clift and Vannucchi*, 2004; *Scholl and von Huene*, 2007]. This is in accordance with our numerical experiments on diapir formation. Strong coupling of the plates promotes sediment subduction and basal erosion of the upper continental crust [*Gerya and Meilick*, 2011; *Vogt et al*., 2012]. Most of the incoming sediments bypass the accretionary wedge, and only small to medium sized prisms are formed. Recent estimates on the net transfer of crustal material on Earth surface suggest that crustal rocks are recycled back into the mantle at the same rate (25–50 km^3/km/Myr) that continental crust is formed [*Von Huene and Scholl*, 1991; *Scholl and von Huene*, 2007]. Consequently, sediments sink into the mantle and intermix with the oceanic crust to form a hybrid tectonic rock mélange (Figures 2 and 3). Natural mélange occurrences comprise highly deformed metasedimentary collages of incipient metamorphism and chaotic hybrid mixtures of peridotite, basalt, and sediment produced at blueschist-amphibolite- or eclogite conditions, formed in forearc to sub-arc regions [*King et al*., 2006 and references therein]. *King et al*. [2006] have argued that mélange formation is an intrinsic process to all subduction zones and that the geochemistry of mélange will impart the strongest control on the geochemistry of metasomatic agents (hydrous fluids, silicate melts, or miscible supercritical liquids) progressing to arc magmatic source regions in the mantle wedge.

[23] Water released due to dehydration reactions of hydrous phases [e.g., *Schmidt and Poli*, 1998] and compaction of the sedimentary layer and hydrothermally altered oceanic crust [e.g., *Peacock*, 1990] enables partial melting of the tectonic rock mélange. According to our results, buoyant diapirs are formed, composed of partially molten sediment and basalt

that detach from the slab, transporting fertile subducted material towards hotter zones of the mantle wedge (Figures 2 and 3). Early on, it was suggested that hydrous partial melting of the oceanic crust (with a quartz eclogite mineralogy at 100–200 km and 700–900°C) results in silicic magmas that rise and react with the overlying peridotitic mantle to produce olivine-pyroxene diapirs, contaminated with the elements enriched in silicic melts [*Ringwood and Green*, 1966, *Green*, 1980, *Ringwood*, 1989). Later on, phase equilibria and trace element partitioning experiments on pelagic red clay at conditions appropriate to the slab beneath arc volcanoes have demonstrated that sediment melting is required for critical elements (Th and Be) to be transferred to the arc [*Plank*, 2005; *Plank and Langmuir*, 1998; *Johnson and Plank*, 1999). In addition to this, *Skora and Blundy* [2010] have suggested that serpentine breakdown at sublithospheric depth (100 km, 800°C) may enable high degree melting (~54% melt) of sedimentary rocks (i.e., radiolarian clay) by a process coined "flush melting," in contrast to fluid absent melting, which yields negligible melt fraction (<10%) [*Skora and Blundy*, 2010]. This led *Tamura et al*. [2011] to propose that such hydrous sediment melt may mix with the overlying mantle to form a crystal-liquid mush (diapir) that is sufficiently buoyant to initiate diapiric ascent, upon which equilibrium between the crystals and the liquid will be maintained over the changing pressure-temperature conditions.

[24] Recent studies on the density structure of subducted sediments demonstrate that during sediment subduction and sediment erosion more silica-rich rocks are transformed into felsic gneisses that are less dense than the peridotite mantle [*Behn et al*., 2011; *Hacker et al*., 2011; *Miller and Behn*, 2012]. These felsic gneisses can relaminate to the base of the crust, whereas mafic rocks become eclogite and may sink into the mantle [*Hacker et al*., 2011]. Xenoliths of subducted crustal origin from the Pamir Mountains display natural examples of this process [*Ducea et al*., 2003; *Hacker et al*., 2005].

[25] The depth and temperature at which sedimentary layers detach from the downgoing slab have repeatedly been reported to vary between 40–100 km and 500–850°C [*Behn et al*., 2011; *Hacker et al*., 2011; *Miller and Behn*, 2012], which is in accordance with our study. The timescales over which these instabilities grow depend on the viscosity contrast between the sedimentary layer and overlying mantle, temperature, buoyancy, and thickness of the sedimentary layer but are generally believed to be rapid <3 Myr [*Behn et al*., 2011; *Miller and Behn*, 2012]. Analog studies on diapiric flow at subduction zones have moreover indicated that the interaction between buoyantly upwelling diapirs and subduction induced flow in the mantle creates a network of low-density, low-viscosity conduits through which flow is rapid [*Hall and Kincaid*, 2001]. Timescales over which such diapiric structures may transverse from the slab (at 70 km depth) to the surface have been estimated to vary between 10^4 to 6×10^6 years [*Hall and Kincaid*, 2001] and are comparable to our results on translithospheric diapirs ($1–5 \times 10^6$ years).

[26] Although there is growing evidence for crustal relamination of subducted material to the base of the continental crust [e.g., *Ringwood*, 1989; *Gerya et al*., 2004; *Gerya and Meilick*, 2011; *Hacker et al*., 2011; *Behn et al*., 2011, *Tamura et al*., 2011], transport mechanisms remain controversial. *Kelemen et al*. [2003a] suggest andesitic melt percolation along low viscosity conduits, while *Behn et al*. [2011] assume buoyant ascent of small 3–4 km sized diapirs, in contrast to the large (5–30 km) diapiric structures proposed by *Gerya and Yuen* [2003]. The transport of andesitic melt through a network of conduits [*Kelemen et al*., 2003a] is compatible with our study. However, we argue that hydrous melting of basalt and sediment along the slab interface may give rise to composite diapirs of granodioritic composition that can relaminate the continental crust, having a strong impact on the petrological and geochemical evolution of the continental crust. Some of these consequences are discussed below. However, further studies on the chemical composition of rock mélange in terms of phase relation and chemical partitioning are necessary to capture its significance in relation to large-scale crustal recycling.

4.2. Diapir Composition and Melt Generation

[27] Trace elements that form the sediment melt signature of arc lavas are believed to retain in the sediments until the rocks have experienced temperatures exceeding 1050°C [*Behn et al*., 2011]. Melting experiments on basaltic and sedimentary components at temperatures exceeding 1000°C show that tectonic rock mélange are favorable for the production of granodioritic liquids [*Castro and Gerya*, 2008; *Castro et al*., 2010]. However, these temperatures are higher than those at the slab surface (700–900°C), where according to our studies composite diapirs assemble and form before they finally detach from the slab [*Gerya and Meilick*, 2011; *Vogt et al*., 2012]. This led *Behn et al*. [2011] to conclude that, although sediment

melting may commence at lower temperature, the key elements associated with the sediment melt signature are not released until temperatures exceed 1050°C and to propose that sediments detach from the slab to undergo dehydration melting in the hot mantle wedge. However, our models show that in spite of the intense heat exchange between the ascending diapir and the hot asthenosphere, temperatures inside the diapir rarely exceed 1050°C, implying that the rapid ascent outgrows the timescales of thermal diffusion. Alternatively, basaltic melt formed atop the slab at temperatures greater than 1000°C may propagate and interact with the ascending diapir, increasing its temperature and changing its chemical composition. Because of its low viscosity, basaltic melt is expected to move significantly faster than the diapir itself, but further studies on coupled fluid flow are necessary to verify these assumptions. Nevertheless, hybridization of slab-derived melts is strongly supported in terms of experimental phase relations and geochemical mixing line patterns [*Carroll and Wyllie*, 1989; *Johnston and Wyllie*, 1989; *Rapp et al*., 1999, *Chauvel et al*., 2008]. Recent laboratory experiments on MORB-Greywacke and Spinellherzolite of *Castro et al*. [2012a] have demonstrated that reactions between these components produce andesitic melt with magnesium numbers (MgO/MgO/FeO = 0.6), typical for rocks of the continental crust [*Kelemen*, 1995].

[28] The compositional variations of the parental magma (diapir) shown in this study are limited to X_b = 04–0.8 (Figures 4a and 5a), which according to *Castro et al*. [2010] is favorable for the production of granodioritic melt. While partial melts of the end-members—sediments and basalts—form granitic and trondhjemitic melts, respectively, mixtures of sedimentary and basaltic components are buffered by the coexisting solid assemblage and are likely to produce granodioritic melt if X_b is limited to 0.25–0.75 [*Castro et al*., 2012a]. This melt may hybridize with basaltic melt, formed by partial melting of the hydrated mantle, reheat and form High-Mg, low-silica andesite magmas. The compositional variations of the parental magma (X_b) are related to material inputs at the slab interface. This results in magmatic pulses that are transferred to crustal levels and may represent different magma batches. Many batholiths formed along the western coast of North and South America show, despite their long-lived magmatic activity over tens of millions of years, evidence for cyclical growth [*DeCelles et al*., 2009] by episodically intruded magma pulses [e.g., *Pankhurst et al*., 1999, *Hervé et al*., 2007]. During emplacement, diapirs may segregate into solid residues and melt, contributing to the generation of granulites in the lower crust and silicic melt at upper crustal levels that may form batholiths and dacitic volcanism [*Castro et al*., 2012a]. Hence, composite diapirs may be an efficient mechanism by which granodioritic melt is produced and transported.

4.3. Pressure-Temperature Evolution of the Melting Zone

[29] We have traced the pressure-temperature evolution of 16 different rocks (tracers in the 2D domain) from the translithospheric and underplating diapir shown in Figures 2 and 3. The red dots in Figure 6 represent partially molten rocks within the diapir that have been traced through time. There is a significant difference between the thermal evolution of translithospheric (Figures 6a and 6b) and underplating diapirs (Figures 6c and 6d). While translithospheric diapirs ascend rapidly to cooler regions after reaching peak temperatures of 800–1000°C (Figures 6a and 6b), partial melting of underplating diapirs occurs mainly within the hot region of the mantle (15–20 kbar) at temperatures of around 1000° C (Figures 6c and 6d). Because of the strong continental lithosphere, underplating diapirs cannot penetrate towards shallower levels and spread along the lithospheric base, where they remain for long periods of time (20 Myr). Although melting may commence at lower temperatures (~800°C), most of the material melts at temperatures of around 1000°C that prevail at the base of the lithosphere (Figure 6d). Translithospheric diapirs, on the other hand, move quickly towards shallower crustal levels and are characterized by the recurrent supply of new magma, forming distinct magma batches. Hence, melting occurs over a broad range of pressure-temperature conditions (Figure 6a) rather than within a focused region. Once peak temperatures of around 800–1000°C are reached, most of the partially molten material undergoes rapid cooling (Figure 6b) because of the rapid ascend of the diapir. These temperatures (<1000°C) are unlikely to produce water-undersaturated granodioritic melt [*Castro et al*., 2010], but basaltic liquids from the hot mantle wedge may reheat the diapir as they move towards the surface. Partial melting of the hydrated mantle is believed to commence at temperatures exceeding 1000°C [*Kushiro*, 1974; *Green*, 1973; *Niida and Green*, 1999], hence any reaction between ascending hot basaltic melt and the diapir may significantly change its thermal structure. The close spatial association of mantle-derived rocks (gabbros) and granodiorite-tonalite intrusions in most Cordilleran [e.g., Sierra Nevada:

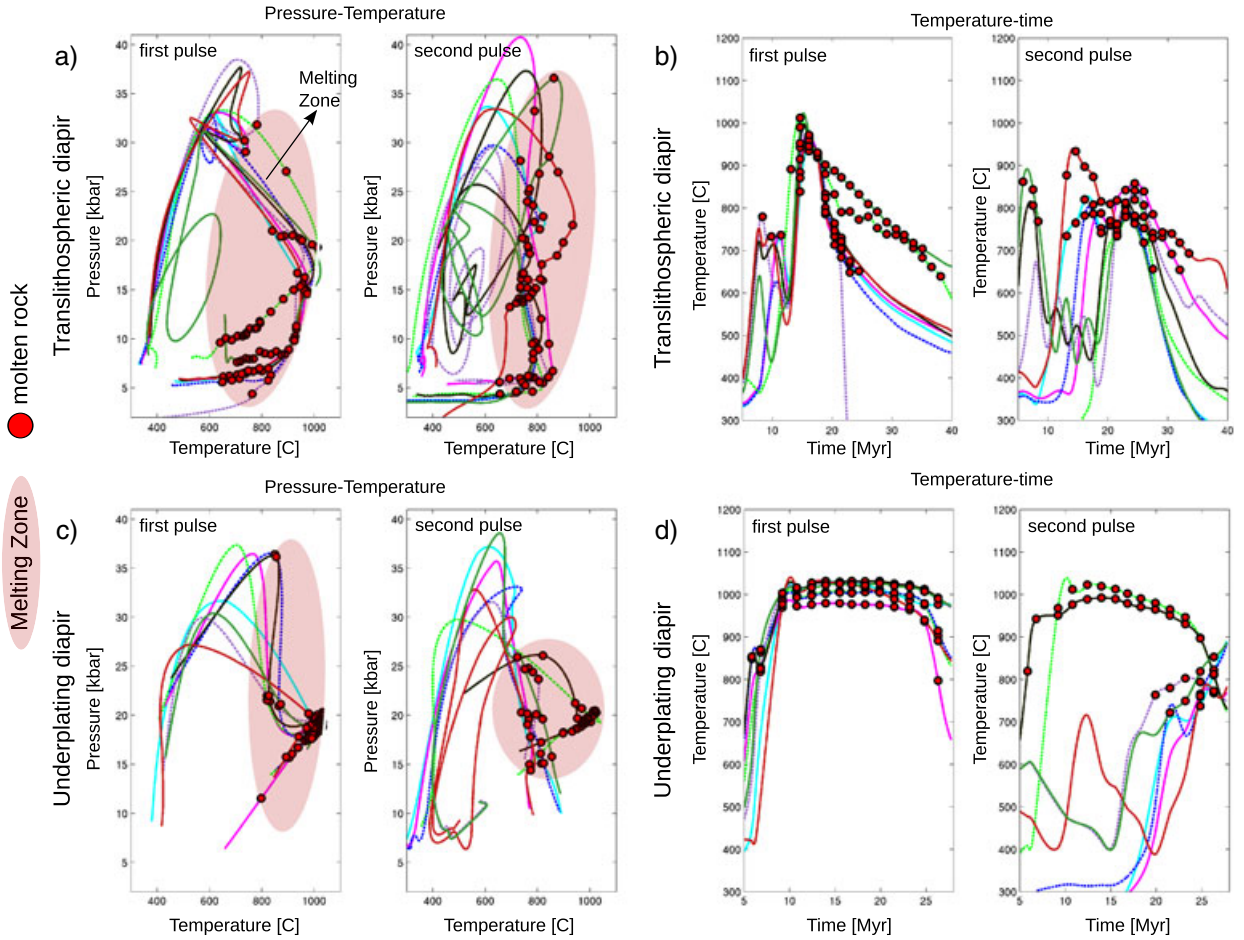

Figure 6. Thermodynamic constraints on the melting zone showing pressure-temperature conditions of 16 rocks that have been traced during the simulation. The dashed and solid lines represent PT paths of these rocks/tracers. Partially molten rocks are represented by solid red dots. (a) and (b) show the pressure-temperature and temperature-time evolution of rocks from different magma batches of the translithospheric diapir. (c) and (d) show the pressure-temperature and temperature-time evolution of rocks from different magma batches of the underplating diapir. (a) The rapid ascent of crustal material through the mantle results in a broad melting zone. Temperature and pressure vary between 650–1000°C and 2–35 kbar, respectively. (b) After reaching peak temperatures of around 800°C–1000°C, most rocks undergo rapid cooling. (c) Melting occurs mostly within a region of 800–1050°C and 10–25 kbar, which prevails at the base of the lithosphere. (d) Most of the material remains at temperatures of around 1000°C for up to 20 Myr, prior to emplacement.

Lee et al., 2006; *Frost and Mahood*, 1987], pre-Cordilleran [e.g., Famatinan arc: *Castro et al.*, 2012b], and post collisional batholiths [e.g., Spanish Central System: *Bea and Montero*, 1999; European Caledonides: *Stephens*, 1988] suggest a genetic link between mantle-derived sources and crustal components.

4.4. Geochemical Implications

[30] According to experimental data [*Castro et al.*, 2010; 2012a], the major element composition of melt derived from partially molten diapirs is buffered for sediment to MORB ratios, ranging from 3:1 to 1:3, producing melt of granodiorite composition. Geochemical and isotopic variations, on the other hand, will be inherited from a composite source, i.e., diapir. During equilibrium melting, the isotopic features of the solid end-members, i.e., basalt and sediment will be transferred to the liquid. Although isotopic disequilibrium has been reported with regard to Nd isotopes during crustal anatexis [e.g., *Barbero et al.*, 1995], the conditions for mélange melting are more favorable for equilibrium melting because temperatures are expected to be higher and timescales to be larger. Unlike crustal anatexis, where crustal material undergoes rapid cooling after reaching peak temperatures, diapir melting occurs within the hot zone of the mantle,

where partially molten crustal material remains hot for several Myr (Figure 6).

[31] The compositional variations of the parental magma (Figures 4a and 5a), produced by material inputs of differing proportions ($X_b = 04–0.8$), are manifested in the geochemical evolution of the liquid (Figures 4b and 5b). Radiogenic isotopes (Sr, Nd) change with time according to the basalt fraction in the source. For example, an increase in basaltic components (from $X_b = 0.55$ to $X_b = 0.7$) leads to an increase in εNd (from −1 to +2) and a decrease in $^{87}Sr/^{86}Sr$ (from 0.707 to 0.705) values. Hence, the resulting liquid evolves towards a more primitive (isotopic) composition. In contrast, a decrease in basaltic components results in a more evolved composition with increasing $^{87}Sr/^{86}Sr$ and decreasing εNd values (Figures 4b and 5b). Nevertheless, melt extracted from partially molten diapirs may intermix and react with the overlying mantle as it percolates towards the surface. To account for this behavior, we have calculated the isotopic signatures that are expected to evolve by chemical interactions of melt derived from composite diapirs and the perioditic mantle (Figures 4c and 5c). However, hybridization of these liquids with the overlying mantle has little effect on the isotopic characteristics as shown in Figures 4c and 5c because the isotopic initial ratios of the hybrid system (diapir + mantle) are related to the element abundances of Sr and Nd in the components (diapir versus mantle). Crustal diapirs represent strongly fractionated reservoirs, enriched in incompatible elements with Nd and Sr abundances that are an order of magnitude higher compared to the mantle, which is depleted in Sr and Nd (Table 4). Therefore, any reaction of these liquids with the overlying mantle may produce strong enrichment in Mg, forming High Mg andesites, but insignificant modification in terms of radiogenic isotopes (Sr, Nd) that are mostly controlled by the element abundances of incompatible elements. If magma ascent occurs in a common place, this reaction may be even less effective because reaction aureoles may form and prevent further hybridization. Hence, any temporal variation of the parental magma in terms of radiogenic isotopes is transferred to the liquids that may react with the peridotite mantle but will not undergo any essential changes in radiogenic isotopes that are imposed by the parental magma. Emplacement of such composite diapirs at crustal levels may finally lead to crustal assimilation, including partial melting, magma mingling, and crustal anatexis that will influence the isotopic evolution of these magmas but are not considered in this study.

4.5. Implications and Natural Observations

[32] Active continental margins are major sites of magmatism. Silic magmas of intermediate composition form either plutonic intrusions or extrusive volcanics. The former are assembled in form of large batholiths along active continental margins that contribute to the growth and evolution of continental crust [*Condie*, 1997; *Hawkesworth and Kemp*, 2006; *Kemp and Hawkesworth*, 2003]. However, batholiths cannot be derived directly by partial melting of the mantle, and their genesis may involve large amounts of recycled crustal material as evidenced by Nd-Sr isotopic ratios [*Allègre and Ben Othman*, 1980; *McCulloch and Wasserburg*, 1978]. Other characteristic features of calc-alkaline batholiths include (i) the uniformity of major element compositions, (ii) hybrid crust-mantle isotopic signatures, and (ii) significant changes in isotopic signatures with time and space. Although generally believed to have formed by fractionation ("distillation") of hydrous mantle-derived magmas [*Hawkesworth and Kemp*, 2006; *Annen et al*., 2006], batholiths may also form by partial melting of crustal components at sublithospheric depth. For example, *Takagi* [2004] argued based on $^{87}Sr/^{86}Sr$, εNd and δO values of granitic plutons in the Japan Arc that the temporal variation of initial $^{87}Sr/^{86}Sr$ isotope ratios is mainly attributed to source contamination, caused by melting of subducted materials in the mantle source region, rather than to the properties of the lower continental crust, which is in accordance with our study on diapir formation.

[33] Partial melting of composite diapirs produces homogenous liquids of granodioritic composition because compositional variations of the parental magma (diapir) are buffered by the solid residues and are not transferred to the liquids [*Castro et al*., 2010]. In contrast, isotopic and geochemical variations will be inherited from a compositionally heterogenous source, i.e., basalt and sediment (diapir) (Figures 4b 4c, 5b, and 5c). Given the continuous supply of sediment and basalt along the slab, magma supply and melt production may sustain over long periods of time, adding new material of granodioritic composition to the base of the crust with minor changes in major element compositions but substantial variations in radiogenic isotopes.

4.6. Long-time Isotopic Evolution of Batholiths

[34] In some natural geological settings, batholiths evolve towards a more primitive composition in

terms of initial isotopic ratios (decrease in Sr/Sr, increase in εNd), while their major element composition remains constant over hundreds of Myr of years [*Pankhurst et al*., 1999; *Hervé et al*., 2007]. The progressive change from isotopically evolved to isotopically primitive compositions has been explained by the shielding effect of older plutons, resulting in a decrease of crustal contamination of mantle-derived magmas [*Bruce et al*., 1991] or the simultaneous mixing and melting of more primitive components [*Pankhurst et al*., 1999]. However, if assimilation is the cause of compositional variations, a parallel evolution of major element compositions and isotopic patterns is expected because assimilation and magma mixing are not selective processes. Isotopically more evolved rocks (increase in $^{87}Sr/^{86}Sr$ ratio and decrease in εNd) should have higher silica and alkali contents, in comparison to more primitive rocks. However, this is not the case. Granites with identical major element compositions plot in both the mantle-like and crustal-like regions in terms of Sr and Nd initial isotopic ratios (see review in *Castro et al*. [2010]). Therefore, we argue that differences in isotope ratios are inherited from an already hybrid source (rock mélange composed of basalt and sediment), which does not affect the major element composition of melts derived from it.

5. Conclusions

[35] Subduction of oceanic crust and sediments results in the formation of tectonic rock mélanges composed of basalt, sediment, and hydrated / serpentinized mantle. Our numerical experiments suggest that these rock mélanges may evolve into partially molten crustal diapirs that rise through the mantle prior to emplacement at crustal levels (relamination). The proportions of basaltic and sedimentary components in the mélange are limited to short-range variations within an interval of X_b (=volume fraction of basalt/basalt + sediment) = 0.4 – 0.8 and yield granodioritic melt. Melt derived from composite diapirs inherits the geochemical characteristics of the composite source and shows distinct temporal variations of radiogenic isotopes (Sr and Nd) depending on the changing values of X_b in the source. The decoupling between radiogenic isotopes and major elements may explain short-range variations observed in some batholiths along the Andean Cordillera.

Acknowledgment

[36] The manuscript has been improved by comments from Brad Hacker and Vlad C. Manea.

[37] K.V. and T.G. acknowledge financial support from the SNF ProDoc program 4D-Adamello. A.C. acknowledges financial support from Grants P09-RNM-05378 and CGL2010-22022-C02-01

References

Allègre, C. J., and D. Ben Othman (1980), Nd-Sr isotopic relationship in granitoid rocks and continental crust development: A chemical approach to orogenesis, *Nature 286*, 335–341.

Amstrong, R. L. (1981), Radiogenic isotopes: The case for crustal recycling on a near-steady-state no continental-growth Earth, *Phil. Trans. Roy. Soc. Lond. Math. Phys. Eng. Sci.*, *301*(1461), 443–72.

Annen, C., J. D. Blundy, and R. S. J. Sparks (2006), The genesis of intermediate and silicic magmas in deep crustal hot zones, *J. Petrol. 47*, 505–539.

Barbero, L., C. Villaseca, G. Rogers, and P. E. Brown (1995), Geochemical and isotopic disequilibrium in crustal melting: An insight from the anatectic granitoids from Toledo, Spain, *J. Geophys. Res. 100*(B8).

Bea, F., and P. Montero (1999), Behavior of accessory phases and redistribution of Zr, REE, Y, Th, and U during metamorphism and partial melting of metapelites in the lower crust: An example from the Kinzigite Formation of Ivrea-Verbano, NW Italy, *Geochim. Cosmochim. Acta 63*, 1133–1153.

Behn, M. B., P. B. Kelemen, G. Hirth, B. R. Hacker, and H. J. Massonne (2011), Diapirs as the source of the sediment arc signature in arc lavas, *Nat. Geosci.*, DOI: 10.1038/NGEO1214.

Behn, M. D., and P. B. Kelemen (2003), Relationship between seismic P-wave velocity and the composition of anhydrous igneous and meta-igneous rocks, *Geochem.Geophys. Geosyst. 4*, art. no. 1041.

Bittner, D., and H. Schmeling (1995), Numerical modeling of melting processes and induced diapirism in the lower crust, *Geophys. J. Int.*, *123*, 59–70.

Bruce, R. M., E. P. Nelson, S. G. Weaver, and D. R. Lux (1991), Temporal and spatial variation in the south Patagonian batholith: Constraints on magmatic arc development, in *Andean Magmatism and Its Tectonic Setting*, edited by R. S. Harmon, C. W. Rapela, Geological Society of America Special Papers, 265, 1–12.

Carlson, R. L. (2003), Bound water content of the lower oceanic crust estimated from modal analyses and seismic velocities of oceanic diabase and gabbro, *Geophys. Res. Lett. 30*, art. no. 2142.

Carroll, M. R., and P. J. Wyllie (1989), Experimental phase relations in the system tonalite-peridotite-H_2O at 15 kb; implications for assimilation and differentiation processes near the crust-mantle boundary, *J. Petrol.*, *30*, 1351–1382.

Castro, A., and T. V. Gerya (2008), Magmatic implications of mantle wedge plumes: Experimental study, *Lithos*, *103*, 138–148.

Castro, A., J. Diaz-Alvarado, and C. Fernandez (2012a), Fractionation and incipient self-granulitization during deep-crust emplacement of Lower Ordovician Valle Fértil batholith at the Gondwana active margin of South America, *Gondwana Res.*, http://dx.doi.org/10.1016/j.gr.2012.08.011.

Castro, A., A. García-Casco, C. Fernández, L. G. Corretgé, I. Moreno-Ventas, T. Gerya, and I. Löw (2009), Ordovician

ferrosilicic magmas: Experimental evidence for ultrahigh temperatures affecting a metagreywacke source, *Gondwana Res.*, *16*, 622–632.

Castro, A., T. V. Gerya, A. García-Casco, C. Fernández, J. Díaz Alvarado, I. Moreno-Ventas, and I. Löw (2010), Melting relations of MORB-sediment mélanges in underplated mantle wedge plumes. Implications for the origin of cordilleran-type batholiths. *J. Petrol. 51*, 1267–1295.

Castro, A., K. Vogt, and T. Gerya (2012b), Generation of new continental crust by sublithospheric silicic-magma relamination in arcs: A test of Taylor's andesite model, *Gondwana Res.*, http://dx.doi.org/10.1016/j.gr.2012.07.004

Chauvel, C., E. Lewin, M. Carpentier, N. T. Arndt, and J.-C. Marini (2008), Role of recycled oceanic basalt and sediment in generating the Hf–Nd mantle array, *Nat. Geosci.*, *1*, 64–67.

Christensen, N. I., and W. D. Mooney (1995), Seismic velocity structure and composition of the continental crust: A global view. *J. Geophys. Res.*, *10*, 9761–9788.

Clauser, C., and E. Huenges (1995), Thermal conductivity of rocks and minerals, in *Rock Physics and Phase Relations. AGU Reference Shelf 3*, edited by T. J. Ahrens, American Geophysical Union, Washington, DC, 105–126.

Clift, P., and P. Vannucchi (2004), Controls on tectonic accretion versus erosion in subduction zones: Implications for the origin and recycling of the continental crust, *Rev. Geophys.*, *42*, RG2001, doi:10.1029/2003RG000127.

Cloos, M., and R. L. Shreve (1988), Subduction-channel model of prism accretion, melange formation, sediment subduction, and subduction erosion at convergent plate margins: 2. Implications and discussion, *Pure Appl. Geophys. 128*, 501–545.

Condie, K. C. (1997), *Plate Tectonics and Crustal Evolution*. Butterworth-Heinemann, Oxford.

Connolly, J. A. D. (2005), Computation of phase equilibria by linear programming: A tool for geodynamic modeling and its application to subduction zone decarbonation, *Earth Planet. Sci. Lett. 236*, 524–541.

Currie, C. A., C. Beaumont, and R. S. Huismans (2007), The fate of subducted sediments: A case for backarc intrusion and underplating, *Geology*, *35*, 1111–1114.

DeBari, S. M., and N. H. Sleep (1991), High-Mg, low-Al bulk composition of the Talkeetna island arc, Alaska: Implications for primary magmas and the nature of arc crust, *Geol. Soc. Am. Bull. 103*, 37–47.

DeCelles, P. G., M. N. Ducea, P. Kapp, and G. Zandt (2009), Cyclicity in Cordilleran orogenic systems, *Nat. Geosci. 2*, 251–257.

Defant, M. J., and M. S. Drummond (1990), Derivation of some modern arc magmas by melting of young subducted lithosphere, *Letters to Nature 347*, 662–665.

Drummond, M. S., and M. J. Defant (1990), A model for trondhjemite-tonalite-dacite genesis and crustal growth via slab melting: Archean to modern comparisons, *J. Geophys. Res. 95*, 21503–21521.

Ducea, M. N., V. Lutkov, V. T. Minaev, B. R. Hacker, L. R. Ratschbacher, P. Luffi, G. E. Gehrels, J. Vervoort, M. O. McWilliams, and J. Metcalf (2003), Building the Pamirs: The view from the underside. *Geology*, *31*, 849–852.

Faure, G. (2001), *Origin of Igneous Rocks. The Isotopic Evidence*. Springer, Berlin-Heidelberg, 496 pp.

Frost, T. P., and G. A. Mahood (1987), Field, chemical, and physical constraints on mafic-felsic magma interaction in the Lamarck Granodiorite, Sierra Nevada, California, *Geol. Soc. Am. Bull. 99*, 272–291.

Gerya, T. V., J. A. D. Connolly, D. A. Yuen, W. Gorczyk, and A. M. Capel (2006), Sesmic implications of mantle wedge plumes, *PEPI*, *156*, 59–74.

Gerya, T. V., and F. I. Meilick (2011), Geodynamic regimes of subduction under an active margin: Effects of rheological weakening by fluids and melts, *J. Metamorph. Geol. 29*, 7–31.

Gerya, T. V., and D. A. Yuen (2003), Characteristics-based marker-in-cell method with conservative finite-differences schemes for modeling geological flows with strongly variable transport properties, *Phys. Earth Planet. In. 140*, 293–318.

Gerya, T. V., and D. A. Yuen (2007), Robust characteristics method for modelling multiphase visco-elasto plastic thermo-mechanical problems. *Phys. Earth Planet. In. 163*, 83–105.

Gerya, T. V., D. A. Yuen, and E. O. D. Sevre (2004), Dynamical causes of incipient magma chambers above slabs. *Geology*, *32*, 89–92.

Gorczyk, W., A. P. Willner, T. V. Gerya, J. A. D. Connolly, and J.-P. Burg (2007), Physical controls of magmatic productivity at Pacific-type convergent margins: Numerical modelling, *Phys. Earth Planet. In. 163*, 209–232.

Green, D. H. (1973), Experimental studies on a model upper mantle composition at high pressure under water-undersaturated and water-saturated conditions, *Earth Planet. Sci. Lett. 19*, 37–53.

Green, T. H. (1980), Island arc and continent-building magmatism—review of petrogenic models based on experimental petrology and geochemistry, *Tectonophysics 63*, 367–385.

Hacker, B. R., P. B. Kelemen, and M. D. Behn (2011), Differentiation of the continental crust, *Earth Planet. Sci. Lett.*, *307*, 501–516.

Hacker, B. R., P. Luffi, V. Lutkov, V. T. Minaev, L. R. Ratschbacher, T. Plank, M. N. Ducea, A. E. Patino-Douce, M. O. McWilliams, and J. Metcalf (2005), Near-ultrahigh pressure processing of continental crust: Miocene crustal xenoliths from the Pamir. *J. Petrol.*, *46*, 1661–1687.

Hall, P. S., and C. Kincaid (2001), Diapiric flow at subduction zones: A recipe for rapid transport. *Science*, *292*, 2472–2475.

Hart, S. R., A. Zindler (1986), In search of a bulk-earth composition. *Chem. Geol. 57*, 247–267.

Haschke, M., W. Siebel, A. Günther, and E. Scheuber (2002), Repeated crustal thickening and recycling during the Andean orogeny in north Chile (21°–26°S). *J. Geophys. Res.*, *107*, 10.1029/2001JB000328

Hawkesworth, C. J., and A. I. S. Kemp (2006), Evolution of the continental crust. *Nature 443*, 811–817.

Hervé, F., R. J. Pankhurst, C. M. Fanning, M. Calderon, and G. M. Yaxley (2007), The South Patagonian batholith: 150 my of granite magmatism on a plate margin. *Lithos 97*(3–4), 373–394.

Hess, P. C. (1989). *Origin of Igneous Rocks*, Harvard University Press, London, UK.

Hildreth, W., and S. Moorbath (1988), Crustal contributions to arc magmatism in the Andes of Central Chile, *Contrib. Mineral. Petrol.*, *98*, 455–489.

Hirschmann, M. M. (2000), Mantle solidus: Experimental constraints and the effects of peridotite composition, *Geochem. Geophys. Geosyst.*, *1*, doi:10.1029/2000GC000070.

Hofmann, A. W. (1988), Chemical differentiation of the Earth: The relationship between mantle, continental crust, and oceanic crust, *Earth Planet. Sci. Lett.*, *9*, 297–314.

Hofmeister, A. M. (1999), Mantle values of thermal conductivity and the geotherm from phonon lifetimes, *Science 283*, 1699–1706.

Iwamori, H. (1998), Transportation of H_2O and melting in subduction zones, *Earth Planet. Sci. Lett. 160*, 65–80.

Johannes, W. (1985). The significance of experimental studies for the formation of migmatites, in *Migmatites*, edited by J. R. Ashworth, pp. 36–85. Blackie, Glasgow, UK.

Johnson, M. C., and T. Plank (1999), Dehydration and melting experiments constrain the fate of subducted sediments, *Geochem. Geophys. Geosyst. 1*, doi: 1999GC000014

Johnston, A. D., and P. J. Wyllie (1989), The system tonalite-peridotite-H_2O at 30 kbar, with applications to hybridization in subduction zone magmatism, *Contrib. Mineral. Petrol.*, *102*, 257–264.

Kay, R. W., and S. M. Kay (1991), Creation and destruction of the lower continental crust, *Geologische Rundschau 80*, 259–278.

Kelemen, P. B., G. M. Yogodzinski, and D. W. Scholl (2003a), Along-strike variation in the Aleutian Island arc: Genesis of high Mg# andesite and implications of continental crust, *Am. Geophysical Union Geophys. Monogr. 138*, 223–276.

Kelemen, P. (1995), Genesis of high Mg# andesites and the continental crust, *Contrib. Mineral. Petrol. 120*, 1–19.

Kelemen, P. B., K. Hanghøj, and A. Greene (2003b), One view of the geochemistry of subduction-related magmatic arcs, with an emphasis on primitive andesite and lower crust, in *The Crust*, edited by H. D. Holland, K. K. Turekian, and R. L. Rudnick, Treatise on Geochemistry Vol. *3*, pp. 593–659, Elsevier Pergamon, Oxford.

Kemp, A. I. S., and C. J. Hawkesworth (2003). Granitic perspectives on the generation and secular evolution of the continental crust, in *The Crust*, edited by R. L. Rudnick, pp. 349–410, Elsevier, Amsterdam.

King, R. L., G. E. Bebout, T. Moriguti, and E. Nakamura (2006), Elemental mixing systematics and Sr-Nd isotope geochemistry of mélange formation: Obstacles to identification of fluid sources to arc volcanics. *Earth Planet. Sci. Lett.*, *246*, 288–304.

Klein, E. M. (2003), Geochemistry of the igneous oceanic crust, in *The Crust*, edited by R. L. Rudnick, pp. 433–463, Treatise on Geochemistry, Elsevier-Pergamon, Oxford.

Kushiro, I. (1974), Melting of hydrous upper mantle and possible generation of andesitic magma: An approach from synthetic systems, *Earth Planet. Sci. Lett. 22*, 294–299.

Lee, C. T. A., X. Cheng, and U. Horodyskyj (2006), The development and refinement of continental arcs by primary basaltic magmatism, garnet pyroxenite accumulation, basaltic recharge and delamination: Insights from the Sierra Nevada, California, *Contrib. Mineral. Petrol. 151*, 222–242.

Levander, A., and M. S. Miller (2012), Evolutionary aspects of the lithosphere discontinuity structure in the Western U.S., *G-cubed*, *13*(1).

Mamani, M., G. Wörner, and T. Sempere (2010), Geochemical variations in igneous rocks of the Central Andean orocline (13°S to 18°S): Tracing crustal thickening and magma generation through time and space. *Geol. Soc. Am. Bull.*, *122*, 162–182.

McCulloch, M. T., and G. J. Wasserburg (1978), Sm-Nd and Rb-Sr chronology of continental crust formation, *Science 200*, 1003–1011.

Miller, N. C., and M. D. Behn (2012), Timescales for the growth of sediment diapirs in subduction zones. *Geophys. J. Int.*, *190*, 1361–1377.

Niida, K., and D. H. Green (1999), Stability and chemical composition of pargasitic amphibole in MORB pyrolite under upper mantle conditions, *Contrib. Mineral. Petrol. 135*, 18–40.

Pankhurst, R. J., S. D. Weaver, F. Herve, and P. Larrondo (1999), Mesozoic-Cenozoic evolution of the North Patagonian Batholith in Aysen, southern Chile, *J. Geol. Soc. 156*(4), 673–694.

Peacock, S. A. (1990), Fluid processes in subduction zones, *Science 248*, 329–337.

Plank, T. (2005), Constraints from thorium/lanthanum on sediment recycling at subduction zones and the evolution of the continents, *J. Petrol. 46*, 921–944.

Plank, T., and C. H. Langmuir (1998), The chemical composition of subducting sediment and its consequences for the crust and mantle, *Chem. Geol. 145*, 325–394.

Poli, S., and M. W. Schmidt (2002), Petrology of subducted slabs, *Annu. Rev. Earth Planet. Sci.*, *30*, 207–237.

Ranalli, G. (1995), *Rheology of the Earth*, Chapman and Hall, London.

Rapp, R. P., N. Shimizu, M. D. Norman, and G. S. Applegate (1999), Reaction between slab derived melts and peridotite in the mantle wedge: Experimental constraints at 3.8 Gpa, *Chem. Geol.*, *160*, 335–356.

Ringwood, A. E. (1989), Slab-mantle interactions: 3. Petrogenesis of intraplate magmas and structure of the upper mantle. *Chem. Geol. 82*, 187–207.

Ringwood, A. E., and D. H. Green (1966), An experimental investigation of the gabbro-eclogite transformation and some geophysical implications, *Tectonophysics 3*, 383–427.

Rogers, G., and Hawkesworth, C. J. (1989), A geochemical traverse across the North Chilean Andes: Evidence for crust generation from the mantle wedge, *Earth Planet. Sci.*, *91*, 271–285.

Rudnick, R. L. (1995), Making continental crust, *Nature 378*, 571–577.

Schmeling H., A. Babeyko, A. Enns, C. Faccenna, F. Funiciello, T. Gerya, G. Globalek, S. Grigull, B. Kaus, G. Morra, and J. van Hunen (2008), A benchmark comparison of spontaneous subduction models—toward a free surface, *Phys. Earth Planet. In. 171*, 198–223.

Schmidt, M. W., and S. Poli (1998), Experimentally based water budgets for dehydrating slabs and consequences for arc magma generation, *Earth Planet. Sci. Lett. 163*, 361–379.

Scholl, D. W., and R. von Huene (2007). Crustal recycling at modern subduction zones applied to the past—issues of growth and preservation of continental basement, mantle geochemistry, and supercontinent reconstruction, in *4D Framework of Continental Crust*, edited by J. Robert, D. Hatcher, M. P. Carlson, J. H. McBride, J. R. M. Catalán, Geological Society of America, vol. *200*, pp. 9–32, Memoir: Geological Society of America, Boulder.

Skora, S. E., and J. D. Blundy (2010), High-pressure hydrous phase relations of Radiolarien clay and implications for the involvement of subducted sediment in arc magmatism. *J. Petrol.*, *51*(11), 2211–2243.

Staudigel, H., S. Hart, H. Schmincke, and B. Smith (1989), Cretaceous ocean crust at DSDP sites 417–418: Carbon uptake from weathering versus loss by magmatic outgassing. *Geochim. Cosmochim. Acta 53*, 3091–3094.

Stephens, W. E. (1988), Granitoid plutonism in the Caledonian orogen of Europe, in *The Caledonian-Appalachian Orogen*, edited by A. L. Harris, D. J. Fettes, Geol Soc London Spec Publ, vol. *38*, 389–404.

Stern, C. R. (1991). Role of subduction erosion in the generation of Andean magmas. *Geology*, *19*, 78–81.

Sun, S. S., and McDonnough, W. F. (1989), Chemical and isotopic systematics of oceanic basalts: Implications for mantle composition and processes, Geological Society, London, Special Publications, vol. *42*, 313–345.

Takagi, T. (2004), Origin of magnetite- and ilmenite-series granitic rocks in the Japan arc, *Am. J. Sci.*, *304*, 169–202.

Tamura, Y., O. Ishizuka, R. J. Stern, H. Shukuno, H. Kawabata, R. W. Embley, Y. Hirahara, Q. Chang, J.-I. Kimura, A. Nunokawa, and S. H. Bloomer (2011), Two primary basalt magma types from Northwest Rota-1 Volcano, Mariana Arc

and its mantle diapir or mantle wedge plume, *J. Petrol.*, *52*(6), 1143–1182.

Tatsumi, Y. (2005), The subduction factory: How it operates in the evolving earth, *GSA Today 15*, no. 7.

Taylor, S. R., and S. M. McLennan (1985), *The Continental Crust: Its Composition and Evolution*, Blackwell, Melbourne.

Turcotte, D. L., and G. Schubert (2002), *Geodynamics*, Cambridge University Press, Cambridge, UK.

Ueda, K., T. Gerya, S. V. Sobolev (2008), Subduction initiation by thermal-chemical plumes, *Phys. Earth Planet. In. 171*, 296–312.

Vogt, K., T. V. Gerya, and A. Castro (2012), Crustal growth at active continental margins: Numerical modeling, *Phys. Earth Planet. In.*, *192–193*, 1–20.

Von Huene, R., and S. Lallemand (1990). Tectonic erosion along the Japan and Peru convergent margins, *Geol. Soc. Am. Bull.*, *102*, 704–720.

Von Huene, R., and D. W. Scholl (1991), Observations at convergent margins concerning sediment subduction, subduction erosion, and the growth of continental crust, *Rev. Geophys.*, *29*, 279–316.

Zhu, G., T. V. Gerya, S. Honda, P. J. Tackley, and D. A. Yuen (2011a), Influences of the buoyancy of partially molten rock on 3-D plume patterns and melt productivity above retreating slabs, *Phys. Earth Planet. In.*, *185*, 112–121.

Zhu, G., T. V. Gerya, D. A. Yuen, S. Honda, T. Yoshida, and J. A. D. Connolly (2009), Threedimensional dynamics of hydrous thermal-chemical plumes in oceanic subduction zones, *Geochem. Geophys. Geosyst. 10*(11).

Zhu, G., T. V. Gerya, and D. A. Yuen (2011b), Melt evolution above a spontaneously retreating subducting slab in a three-dimensional model, *J. Earth Sci.*, *22*, 137–142.